

Condensate Corrosion Behavior of Type 409 Stainless Steel in Simulated Automotive Muffler Environments

P.H. Han¹, Z.H. Xu¹, C.P. Wang¹, M.C. Li^{1,*}, H.Y. Bi^{2,3}

¹ Institute of Materials, School of Materials Science and Engineering, Shanghai University, 149 Yanchang Road, Shanghai 200072, China

² Stainless Steel Technical Centre, Research Institute, Baoshan Iron & Steel Co., Ltd., 580 Changjiang Road, Shanghai 200431, China

³ State Key Laboratory of Development and Application Technology of Automotive Steels (Baosteel Group), 885 Fujin Road, Shanghai 201900, China

*E-mail: mouchengli@shu.edu.cn

Received: 24 February 2014 / Accepted: 21 March 2014 / Published: 14 April 2014

The cyclic method of hot exhaust gas-oxidation and condensates immersion has been adopted to simulate the internal service conditions of automotive mufflers. The condensation corrosion of 409 stainless steel was investigated during the immersion by using electrochemical measurement and surface analysis techniques. Due to the existence of defects, the oxidation and corrosion products layers on the specimen surfaces play an unimportant role in the condensate corrosion. During the cyclic processes, small pits will form gradually and result in relatively steady active corrosion for specimens in the condensate solutions. Trace SO₂ in the hot exhaust gas only exerts slight inhibition on condensate corrosion through the initial oxidation process, but it almost has no influence on condensate corrosion anymore with the progress of cyclic process. The evolution of condensate corrosion is discussed in detail.

Keywords: Automotive exhaust system, Stainless steel, Condensate corrosion, Sulfur dioxide

1. INTRODUCTION

The Chinese automotive industry has been developing rapidly in recent years. There are more and more corrosion issues emerged during warranty periods, which have attracted attention from both car makers and customers. Due to the cyclic condensation and oxidation of exhaust gases, the components such as mufflers of automotive exhaust systems are commonly subjected to corrosion failure [1-4]. It is necessary to clarify the corrosion behavior and improve the corrosion resistance of stainless steels used for exhaust systems.

When the cars meet the long driving trips, the hot exhaust gas may heat the mufflers up to about 400°C, leading to slight thermal oxidation. On the other hand, when they are in short driving trips or frequent run-stop states, exhaust gases will condense easily in the mufflers and other cold end components and induce subsequently condensate corrosion [2,3]. Automotive exhaust gas often contains CO₂, H₂O, O₂, CO, HC, NO_x and SO₂ [5-7]. It is believed that SO₂ plays an important role in the corrosion failure through condensation process, which mainly comes from the sulfur in the fuel. Because low-temperature oxidation will enhance the condensate corrosion of 409 SS [8,9], there is concern if trace SO₂ in the exhaust gas affects further the corrosion resistance of mufflers through its oxidation process. A previous study demonstrated that 500 h of pure oxidation in the SO₂-containing gas gives rise to a little higher corrosion resistance of the oxidized 409 SS [10]. Nevertheless, the condensation of exhaust gas is not considered there, which may change the oxidation process too.

There are some reports on the condensate corrosion of mufflers [1-5,8-11], but the exhaust gas effect on corrosion through the cyclic occurrence of condensation and oxidation is still rare in the literature. In this work, the cyclic exposure of type 409 stainless steel (SS) was conducted in the simulated exhaust gases with or without trace SO₂ and condensate solutions on gasoline engine basis. The purpose is to gain an insight into influence of trace SO₂ in the hot exhaust gases on condensate corrosion of stainless steels for automotive mufflers.

2. EXPERIMENTAL

A commercial Type 409 SS plate was used as test materials and made into specimens with a dimension of 20 × 20 × 1.5 mm. Its chemical composition is given in Table 1, with alloying addition of niobium and titanium [12,13]. A little hole was punched in each specimen for suspension in the oxidation processes. Prior to each experiment, the specimen was ground with 1000 grit waterproof abrasive paper. In order to perform electrochemical measurements during condensates immersions, a thin wire of type 304 SS was welded to the specimen by a point welding machine. The specimen was cleaned finally with ethanol and the welding spot was coated with high temperature inorganic glue.

Table 1. Chemical composition of type 409 stainless steel specimens (wt.%)

Element	C	Si	Mn	P	S	Ni	Cr	N	Ti	Nb
Mass	0.014	0.51	0.22	0.025	0.0012	0.07	11.5	0.008	0.16	0.19

One cyclic experiment includes the following two fundamental steps. The first step is hot exhaust gas-oxidation. The specimen was exposed in simulated exhaust gas at 400°C for 1h and then was taken out and cooled down to room temperature. The second step is condensate immersion. The specimen was half immersed in condensate solution at 80°C for 2h. A total of 30 cycles were performed to reach a relative stable corrosion state.

During the oxidation periods, the specimen was exposed in the synthetic exhaust gas at 400°C, which is the highest working temperature of mufflers. One simulated exhaust gas consists of 10% CO₂, 10% H₂O(g), 0.5% O₂ and 2.5 ppm SO₂ by volume [5,6,10]. As the control, another mixed gas has the same CO₂, H₂O(g) and O₂ contents but no SO₂ (i.e., non-SO₂ environment). H₂O(g) level was controlled by passing pure nitrogen gas through distilled water at the appropriate temperature with a glass bubbler. The immersion tests were carried out in condensate solutions with 1500 ppm SO₄²⁻, 100 ppm Cl⁻ and 50 ppm NO₃²⁻ by weight at 80°C [2,3,9]. The pH value was adjusted to 4 with dilute H₂SO₄ solution to simulate acidic condensates. The temperature of the solution was controlled by water bath. The specimen was half immersed in solution during immersion tests.

Electrochemical measurements were conducted during the immersions at intervals of 5 cycles. Electrochemical corrosion experiments were performed in a three-electrode glass cell containing 200ml condensate solution. In each cycle, the oxidized specimen was half immersed with about 4 cm² in the condensate solution, which served as the working electrode. An Hg/Hg₂SO₄ electrode (MSE) connected to a Luggin capillary was used as the reference electrode and a platinum foil as the counter electrode. Experiments were performed through a PAR (Princeton Application Research, AMETEK, Inc.) system, which comprised an M273A potentiostat / galvanostat, an M5210 lock-in amplifier and the PowerSuite software. Corrosion potential (E_{corr}) was measured from the beginning of immersion for 1h, and electrochemical impedance spectroscopy (EIS) was measured subsequently. During EIS measurement, an alternating current signal with the frequent range from 99 kHz to 0.01Hz and amplitude of 10 mV (rms) was applied on the working electrode at the corrosion potential. EIS spectra were interpreted using the ZSimpWin 3.21 software.

The oxidized and corroded specimens were observed using scanning electron microscopy (SEM) (JSM-6700F). Raman spectrum (Reinshaw inVia Raman microscope) was applied to analyze the phase information on specimen surfaces.

3. RESULTS AND DISCUSSION

3.1 Electrochemical characteristics of condensate corrosion

Fig. 1 gives the variation of corrosion potentials for 409 SS in the condensate solutions with cyclic times of oxidation-immersion tests. At the initial stage of cyclic process, E_{corr} for specimen oxidized in SO₂ environment is often higher than that in non-SO₂ environment. After about 15 cycles, E_{corr} for both specimens reaches the similar values in the range from -770 to -870 mV_{MSE}. As observed from Fig. 1, E_{corr} may fluctuate slightly in the whole cyclic tests, especially before the 7th cycle. These results indicate that the presence of trace SO₂ in the synthetic gas has apparent influence on the initial condensate corrosion through the thermal oxidation, but almost no influence on the long-term corrosion states.

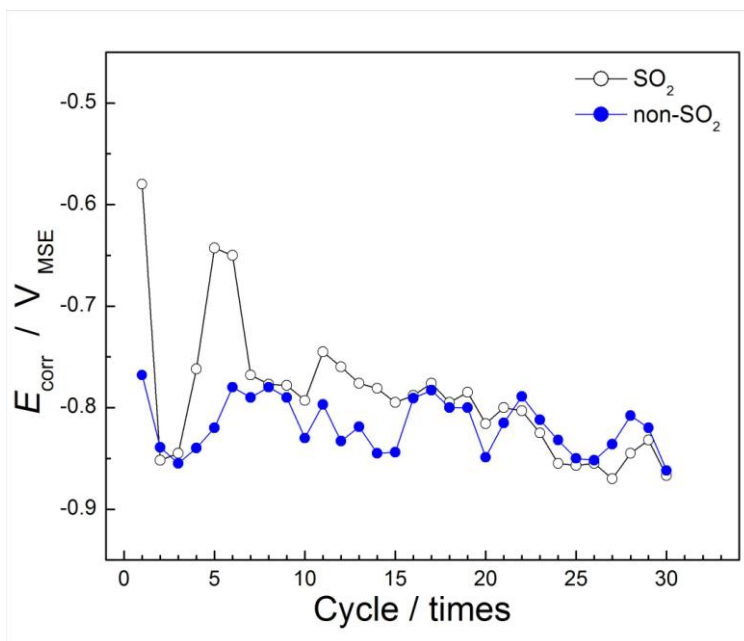


Figure 1. Variation of corrosion potentials for 409 SS in the condensate solutions with cyclic times of oxidation-immersion tests. SO_2 : synthetic gases with SO_2 ; non- SO_2 : synthetic gases without SO_2 .

Fig. 2 shows the complex-plane impedance diagram measured on the specimens after oxidation under both synthetic gas conditions for the first time. Experimental data are also compared with the fitted values obtained from data processing as described later.

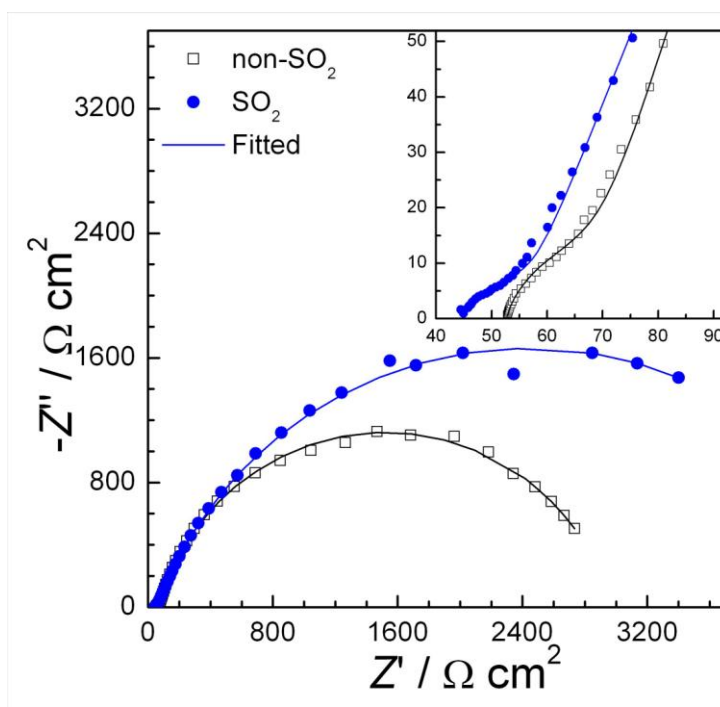
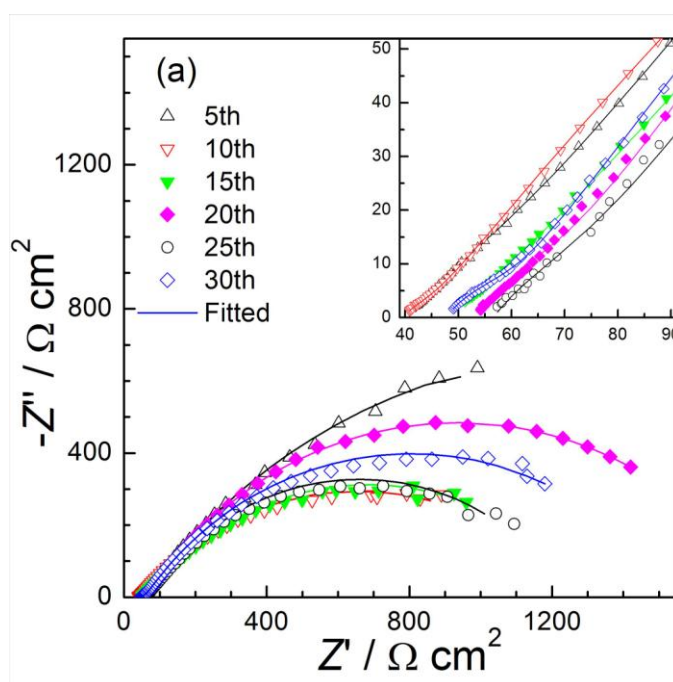


Figure 2. Nyquist plots for 409 SS in the condensate solutions at the first cycle of oxidation-immersion tests. *insets*: the high frequency parts; SO_2 : synthetic gases with SO_2 ; non- SO_2 : synthetic gases without SO_2 .

There is a similar impedance feature for the two types of specimens oxidized in the absence and presence of SO_2 , i.e., two capacitive semicircles over the whole frequency range in Nyquist plots. The high-frequency semicircle can be attributed to the thin oxide films formed on the surface during oxidation process, whereas the low-frequency semicircle results from the charge transfer process [9]. A simple comparison from Fig. 2 indicates that the existence of trace SO_2 leads to a smaller high-frequency semicircle and a larger low-frequency semicircle. It is evident that 409 SS specimens oxidized in the SO_2 environment have higher corrosion resistance than those in the non- SO_2 environment. Because no immersion test is performed before oxidation test, this difference in condensate corrosion is mainly induced by the pure oxidation processes and is consistent with our previous results with 500 h of pure oxidation at 400°C [10].

Fig. 3 gives the impedance plots of specimens in condensate solutions for the 5th to 30th cycle of oxidation-immersion tests under both synthetic gas conditions. The impedance feature at each cycle is similar to that at first cycle in Fig. 2, i.e., being composed of two capacitive semicircles over the whole frequency range. Nevertheless, because the specimens are oxidized in the synthetic gases and immersed in the condensate solutions cyclically, the high-frequency semicircle should be attributed to the thin surface layers of oxidation and corrosion products produced in the cyclic processes. The high-frequency semicircle shrinks or incorporates with the low-frequency semicircle in comparison with that at first cycle and changes insignificantly from the 5th to 30th cycle. The low-frequency semicircles for the specimens oxidized with and without SO_2 shrink noticeably from the 1st to 10th and 15th cycle, respectively, and then expand and fluctuate slightly up to the 30th cycle. These results indicate that the corrosion resistance changes markedly at the initial stage of cyclic tests and reaches relatively stable corrosion state gradually, which are also confirmed by E_{corr} results in Fig. 1. Furthermore, there is no significant difference in the low-frequency semicircle sizes after about 10 cycles of oxidation-immersion tests under both synthetic gas conditions.



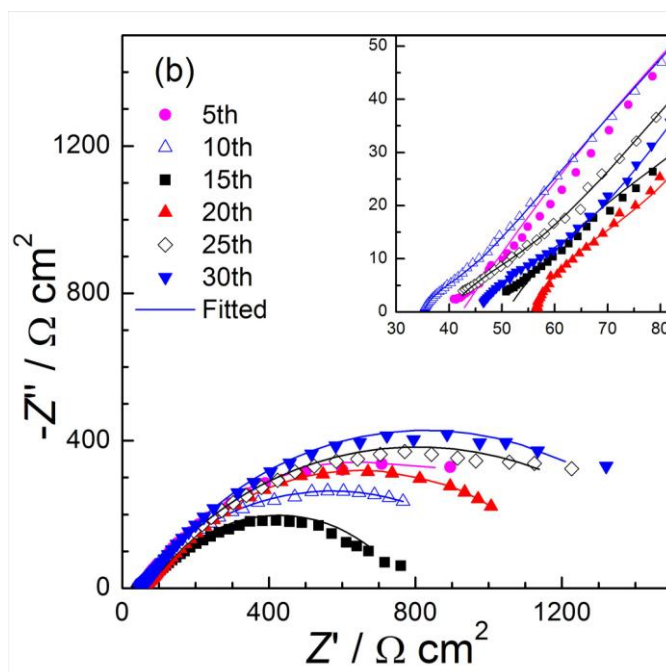
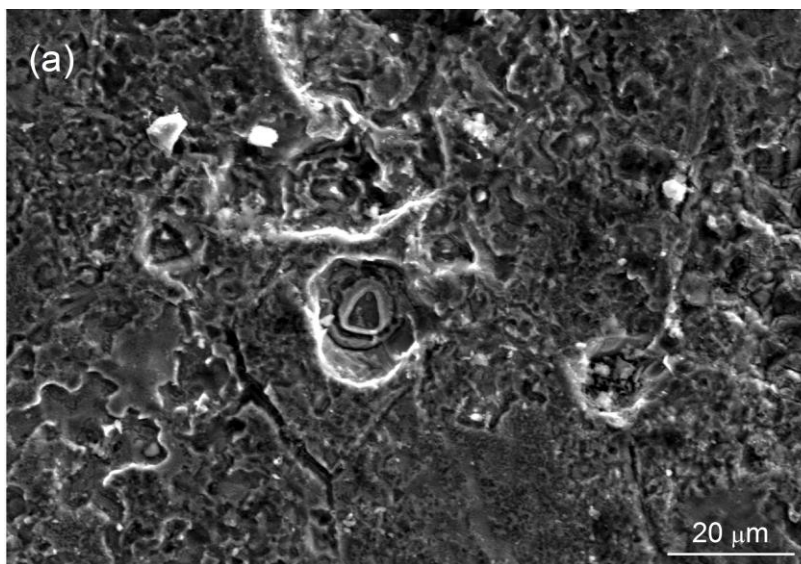


Figure 3. Nyquist plots for 409 SS in the condensate solutions at different cycles of oxidation-immersion tests. (a) synthetic gases with SO₂; (b) synthetic gases without SO₂. *insets:* the high frequency parts.

3.2 Surface morphology and phase analysis

Fig. 4 shows the SEM morphologies of specimens after 30 cycles of oxidation-immersion tests in the presence and absence of SO₂, respectively. It is observed that both specimens are corroded severely after the cyclic processes. The oxidation and corrosion products layers are loose and have some small pits on the surfaces. In general, the morphology of specimen has almost no significant difference between two synthetic gas conditions.



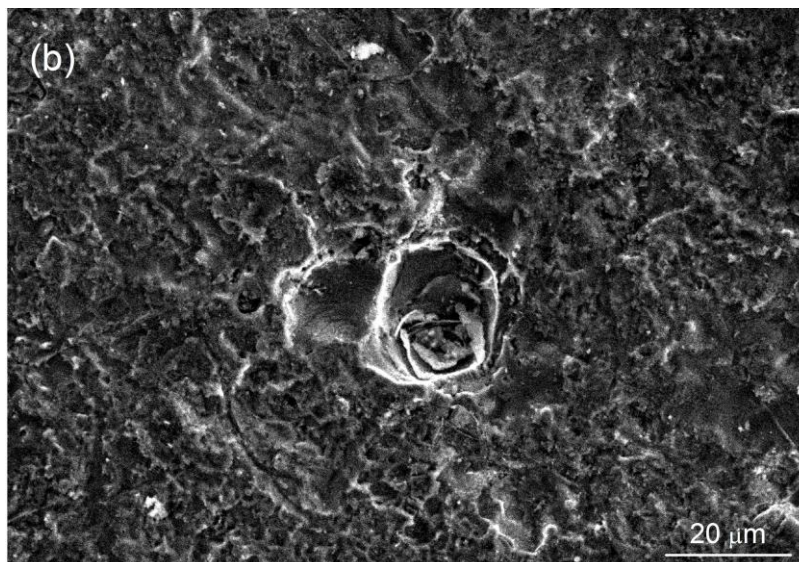


Figure 4. SEM morphologies of specimens after 30 cycles of oxidation-immersion tests under synthetic gas conditions (a) with SO_2 and (b) without SO_2 .

After 30 cycles of experiments, specimen surfaces were analyzed by Raman spectrum, which are shown in Fig. 5. The response peaks are labeled by the corresponding location of intensity maxima. According to the literature [14-17], the weak peak at about 295 cm^{-1} is assignable to $\alpha\text{-Fe}_2\text{O}_3$ (hematite). The peaks at about 670 and 725 cm^{-1} overlap strongly, which maybe result from the mixture of $\gamma\text{-Fe}_2\text{O}_3$ (maghemite), $\beta\text{-FeOOH}$ (akaganite) and some Fe_3O_4 (magnetite). In the condensate solutions without deaeration, dissolved oxygen may behave as an oxidizer to convert Fe_3O_4 into $\beta\text{-FeOOH}$ and/or $\gamma\text{-Fe}_2\text{O}_3$ slowly [18,19].

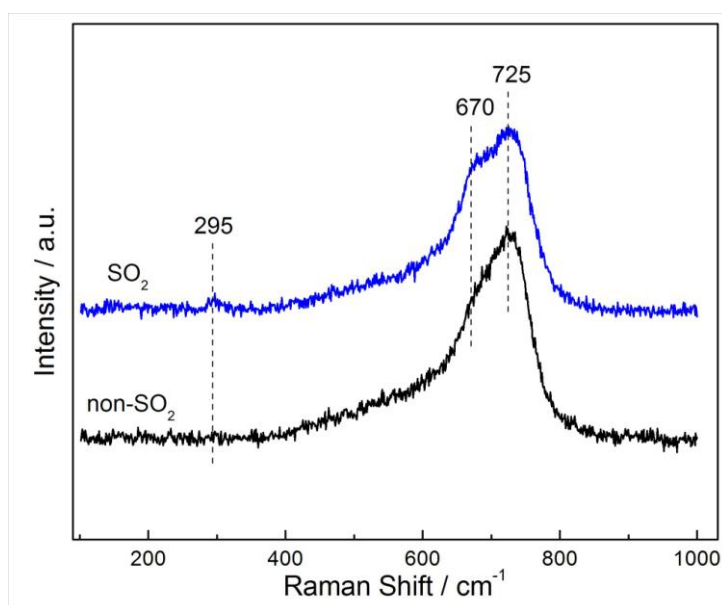


Figure 5. Raman spectra for specimen surfaces after 30 cycles of oxidation-immersion tests. SO_2 : synthetic gases with SO_2 ; non- SO_2 : synthetic gases without SO_2 .

It is apparent that the oxidation and corrosion products layers formed on specimen surfaces under both synthetic gas conditions have a similar phase composition and the same predominant phase β -FeOOH. A further comparison indicates that the peaks at 295 and 670 cm^{-1} are slightly weaker in the non-SO₂ case than in the SO₂ case. This means that the contents of α -Fe₂O₃, γ -Fe₂O₃ and Fe₃O₄ are relatively lower in the surface products layer formed under non-SO₂ condition than under SO₂ condition. In addition, sulfates may form on the specimen surface in the oxidation process with SO₂. But, there is no peak for sulfates in Fig. 5 due to their low contents and/or the dissolution during the cyclic immersion in condensate solutions.

3.3 Interpretation of EIS spectra

On the basis of forming loose products layer of oxidation and corrosion on the specimen surface during the cyclic tests [9,20-22], the electrode system 409 SS/condensate solution in the both synthetic gas cases can be simulated by the equivalent circuit model in Fig. 6. R_s is the electrolyte resistance, R_f and C_f represent the resistance and capacitance of thin products layer on the electrode surfaces, R_t and C_{dl} stand for the charge transfer resistance and double layer capacitance, respectively. In addition, both C_f and C_{dl} were replaced with constant phase element in the fitting procedure due to the non-ideal capacitive response of the corrosion system. As seen in Figs. 2 and 3, the simulated value show good coincidence with the experimental value in spite of the approximations made. This illustrates that the equivalent circuit model provides a reliable description for the condensate corrosion systems in the cyclic processes.

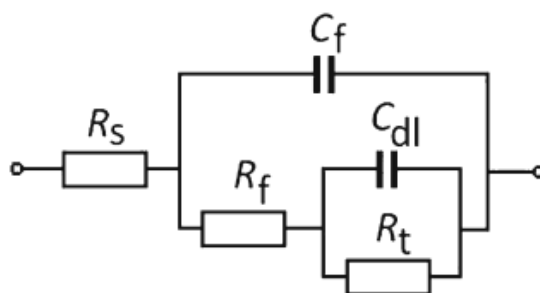


Figure 6. Equivalent circuit for the corrosion system 409 SS/condensate solution

Fig. 7 gives the fitted results of R_f and R_t from EIS spectra for 409 SS specimens under both cyclic test conditions. During the 30 cycles, R_f values are very low and fluctuate slightly in the range 10 to 30 $\Omega \text{ cm}^2$. These imply that the thin products layers on the surfaces play an unimportant role in the condensate corrosion of specimens after oxidation whether the synthetic gas contains trace SO₂ or not. In the range of initial 10 cycles, R_t values decrease greatly, but are much larger in the SO₂ case than in the non-SO₂. After about 10 cycles, R_t values stabilize gradually with slight fluctuations. The stable R_t values are similar and about 1400 $\Omega \text{ cm}^2$ for specimens oxidized in both synthetic gases. These results indicate that the corrosion resistance of each specimen reduces at the initial stage of

cyclic tests, and trace SO_2 in the oxidation environment has an inhibitive effect on the condensate corrosion of oxidized specimens to a certain degree. However, the condensate corrosion may attain relatively steady states subsequently and almost isn't influenced by the presence of trace SO_2 in the oxidation environment.

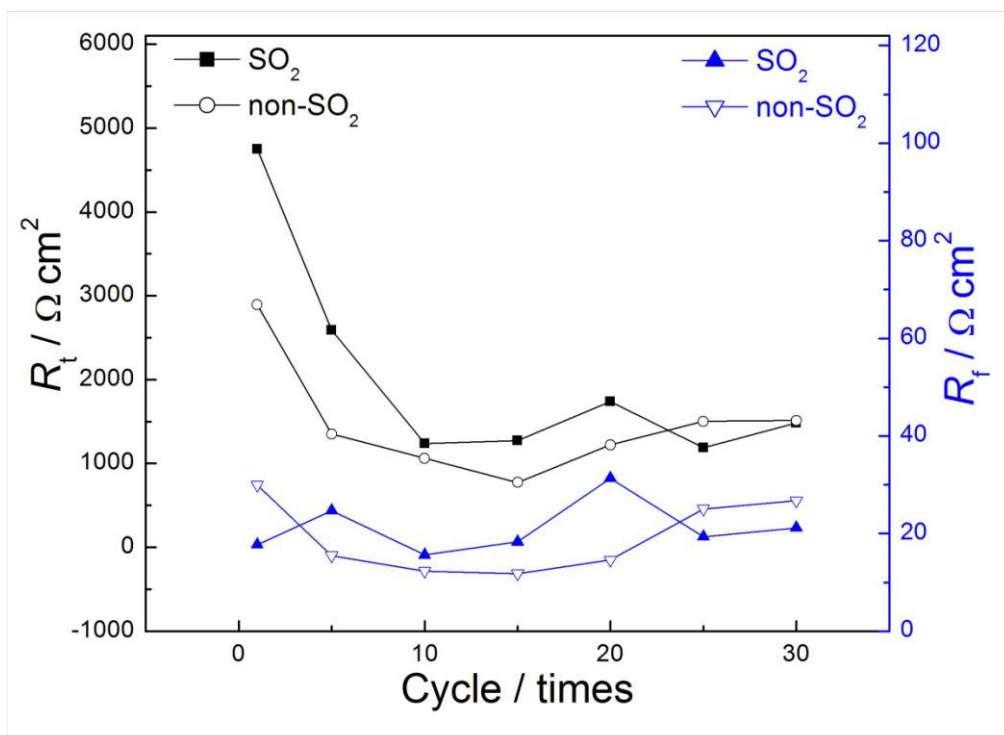


Figure 7. Fitted results of EIS spectra at different cycles for specimens oxidized in the both synthetic gas cases. SO_2 : synthetic gases with SO_2 ; non-SO_2 : synthetic gases without SO_2 .

3.4 Evolution of condensate corrosion

The condensate corrosion of stainless steels in automotive muffler environments involves at least the following aspects: (1) Inhibition of trace SO_2 in the hot exhaust gases on condensate corrosion through thermal oxidation process [10,23,24], (2) Chromium depletion induced by oxidation [8-10], (3) Thin thermal oxide film formed in exhaust gases, (4) Dissolution of thermal oxides in condensate solution [25,26], (5) Corrosion product layer (or passive film), and (6) Active corrosion pits. Above electrochemical behavior of condensate corrosion can be simply interpreted with the effect of these factors and their interactions.

As for the initial corrosion before about 10 cycles under each synthetic gas condition, thin products layer grows slowly in company with occurrence of chromium depletion on the specimen surface. The products layer may also become more defective or porous due to the cyclic dissolution of oxides in condensate solution and oxidation of specimen polluted with condensate ions [9,10], which is confirmed by the rapid decrease of E_{corr} in Fig. 1 and very low R_f values in Fig. 7. These mean that the condensate corrosion depends mostly on the cyclic formation of weak chromium-depleted zone, with insignificant influence of the products layer. Furthermore, the presence of trace SO_2 in the hot

synthetic gases may retard slightly the chromium depletion due to its inhibitive effect on thermal oxidation of 409 SS [10,24]. This is possibly responsible for the higher E_{corr} and larger R_t values in the SO_2 case than in the non- SO_2 case.

After about 10 cycles, the defects in products layer evolve eventually into some small pits on specimen surface because of the progress of cyclic tests. These pits together with the chromium depletion give rise to almost steady active corrosion with low E_{corr} and R_t values as shown in Figs. 1 and 7. At the same time, the loose products layer must accumulate on specimen surface and bring some condensate ions such as SO_4^{2-} and Cl^- into the oxidation process. These ions will accelerate greatly the oxidation process [9,27] and then eliminate the inhibition of trace SO_2 to a great extent. As a result, the steady condensate corrosion has no relation to trace SO_2 in the synthetic gases and shows similar E_{corr} and R_t values under both synthetic gas conditions.

In addition, there are some fluctuations for E_{corr} , R_f and R_t with the increase of cyclic times in Figs. 1 and 7. This can be attributed mainly to the growth of micro-defects in thin oxide films and/or pits on specimen surfaces as well as oxidation repeated at these sites in the cyclic processes.

4. CONCLUSIONS

During the cyclic processes of oxidation in exhaust gases and immersion in condensate solutions, the condensate corrosion resistance of 409 SS decreases initially with increasing the cyclic times and then become stable with the formation of pits on the surface. The pits give rise to steady active condensate corrosion though thermal oxidation takes place repeatedly and results in the fluctuations of corrosion potential and corrosion resistance. The oxidation and corrosion products layers consist mainly of $\alpha\text{-Fe}_2\text{O}_3$, $\gamma\text{-Fe}_2\text{O}_3$, $\beta\text{-FeOOH}$ and some Fe_3O_4 and have insignificant influence on the condensate corrosion due to the existence of defects.

Trace SO_2 in the hot synthetic exhaust gas may inhibit the condensate corrosion of 409 SS through thermal oxidation process during the initial cyclic processes. However, with the progress of cyclic processes, it almost can hardly influence the condensate corrosion anymore, which is attributed mainly to the formation of pits and the marked acceleration effect of condensate ions on the thermal oxidation process. It seems that SO_2 in the exhaust gases facilitates the condensate corrosion of 409 SS only through the condensation process.

ACKNOWLEDGEMENTS

Financial support provided by Natural Science Foundation of China (NSFC, grant no. 51134010) and Specialized Research Fund for the Doctoral Program of Higher Education (20133108110019) is appreciated greatly.

References

1. T. Ujiro, M. Kitazawa, F. Togashi, *Mater. Perform.* 33 (1994) 49-53.
2. Y. Inoue, M. Kikuchi, *Nippon Steel Technical Report*, No. 88 (Jul. 2003), p62-69.

3. J. Douthett, *Automotive Exhaust System Corrosion*, ASM Handbook Volume 13C, Corrosion: Environments and Industries, ASM International, 2006, p519-530.
4. M. Atsushi, H. Junichiro, F. Osamu, *JFE Technical Report*, No. 4 (Nov. 2004), p61-66.
5. J. Nockert, L. Nyborg, M. Norell, *Mater. Corrs.* 63 (2012) 388-395.
6. R.M. Heck, R.J. Farrauto, *Appl. Catal. A: Gen.* 221 (2001) 443-457.
7. P. Engstrom, A. Amberntsson, M. Skoglundh, E. Fridell, G. Smedler, *Appl. Catal. B: Environ.* 22 (1999) L241-L248
8. D. Kim, H. Kim, *J. Kor. Inst. Met. Mater.* 46 (2008) 652-661.
9. M.C. Li, S.D. Wang, R.Y. Ma, P.H. Han, H.Y. Bi, *J. Solid State Electrochem.* 16 (2012) 3059-3067.
10. M.C. Li, H. Zhang, R.F. Huang, S.D. Wang, H.Y. Bi, *Corros. Sci.* 80 (2014) 96-103.
11. R. Hashimoto, G. Mori, M. Yasir, U. Troger, H. Wieser, *BHM* 158 (2013) 377-383.
12. J.A. Cabral-Miramontes, J.D.O. Barceinas-Sanchez, C.A. Poblano-Salas, G.K. Pedraza-Basulto, D. Nieves-Mendoza, P.C. Zambrano-Robledo, F. Almeraya-Calderon, J.G. Chacon-Nava, *Int. J. Electrochem. Sci.* 8 (2013) 564-577.
13. A.S. Hamdy, E. El-Shenawy, T. El-Bitar, *Int. J. Electrochem. Sci.* 1 (2006) 171-180.
14. Q.M. Jin, J. Li, Y.L. Xu, X.S. Xiao, W. Zhang, L.Z. Jiang, *Corros. Sci.* 52 (2010) 2846-2854.
15. T. Kohn, K.J.T. Livi, A.L. Roberts, P.J. Vikesland, *Environ. Sci. Technol.* 39 (2005) 2867-2879.
16. A. Reichmann, P. Poelt, Ch. Brandl, B. Chernev, P. Wilhelm, *Oxid. Met.* 70 (2008) 257-266.
17. D.L.A. de Faria, S. V. Silva, M.T. de Oliveira, *J. Raman Spectrosc.* 28 (1997) 873-878.
18. W.C. Baek, T. Kang, H.J. Sohn, Y.T. Kho, *Electrochim. Acta* 46 (2001) 2321-2325.
19. M.G.S. Ferreira, T. Moura e Silva, A. Catarino, M. Pankuch, C.A. Melendres, *J. Electrochem. Soc.* 139 (1992) 3146-3151.
20. A. Kocijan, D.K. Merl, M. Jenko, *Corros. Sci.* 53 (2011) 776-783.
21. M.C. Li, C.L. Zeng, S.Z. Luo, J.N. Shen, H.C. Lin, C.N. Cao, *Electrochim. Acta* 48 (2003) 1735-1741.
22. S.S. Xin, M.C. Li, *Corros. Sci.* 81 (2014) 96-101.
23. T. Jonsson, A. Jardnas, J.E. Svensson, L.G. Johansson, M. Halvarsson, *Oxid. Met.* 67 (2007) 193-213.
24. A. Jardnas, J.E. Svensson, L.G. Johansson, *Oxid. Met.* 69 (2008) 249-263.
25. T. Zimina, E. Oshe, V. Dubkov, P. Zimin, E. Zabrodskaya, *J. Electrochem. Soc.* 145 (1998) 2236-2240.
26. S. Virtanen, P. Schmuki, A.J. Davenport, C.M. Vitus, *J. Electrochem. Soc.* 144 (1997) 198-204.
27. C.C. Tsaur, J.C. Rock, C.J. Wang, Y.H. Su, *Mater. Chem. Phys.* 89 (2005) 445-453.